Dynamic Downscaling of Seasonal Climate Predictions over Brazil

LEONARD M. DRUYAN AND MATTHEW FULAKEZA

Center for Climate Systems Research, Columbia University Earth Institute, NASA Goddard Institute for Space Studies, New York, New York

PATRICK LONERGAN

Stinger Ghaffarian Technology, Inc., NASA Goddard Institute for Space Studies, New York, New York

(Manuscript received 10 December 2001, in final form 29 April 2002)

ABSTRACT

Climate projections for March–April–May (MAM) 1985 and 1997 made with the NASA Goddard Institute for Space Studies (GISS) GCM over South America on a 4° latitude by 5° longitude grid are ''downscaled'' to 0.5° grid spacing. This is accomplished by interpolating the GCM simulation product in time and space to create lateral boundary conditions (LBCs) for synchronous nested simulations by the regional climate model (RCM) of the GISS/Columbia University Center for Climate Systems Research. Both the GCM and the RCM simulations use sea surface temperature (SST) predictions based on persisted February SST anomalies. Each downscaled prediction is evaluated from an ensemble of five simulations and each is compared to a control ensemble of five RCM simulations driven by synchronous NCEP reanalysis data. An additional five-run control ensemble for MAM 1997 tests the impact of ''perfect'' SST predictions on the RCM forecast. Results are compared to observational evidence that includes NCEP reanalysis data, Climate Prediction Center (CPC) Merged Analysis of Precipitation (CMAP) gridded fields, some rain gauge observations, and satellite measurements of monthly mean outgoing longwave radiation. The downscaled predictions and the downscaled analyses both capture the meridional displacement of the intertropical convergence (ITC) precipitation maximum over northern Brazil between the two seasons. The simulation of this feature for MAM 1997 is improved by using actual SST, but the correction of underestimates of eastern Brazil precipitation requires analyzed LBC in place of GCM forcing. The realism of spatial patterns and area averages of precipitation neither improves nor deteriorates with elapsed time, but the variability between individual runs forced by the same LBC decreases with time. The RCM shows a positive bias in surface temperature over central and southeastern Brazil and a positive bias in temperature at 850 mb over the Tropics. Results imply that improvements in seasonal climate prediction at the 0.5° spatial scale over Brazil could be realized by more realistic GCM forcing, accurate SST predictions, and improvements in the RCM.

1. Introduction

Considerable research has been devoted to statistical prediction of northeast Brazil (Nordeste) seasonal precipitation (Hastenrath 1990; Hastenrath and Greischar 1993) but these empirical approaches require high quality and long series of observations of predictors, some of which represent midoceanic conditions where data quality and availability cannot be assured. Numerical climate simulation models, on the other hand, can supply a rich variety of climate variables at high spatial and temporal resolution. Global circulation models (GCMs) and regional modeling systems also have the advantage of being sensitive to the interannual variability that is related to natural cycles such as El Niño–Southern Oscillation (ENSO) or other sea surface temperature anomalies (SSTAs). Accordingly, sophisticated numerical physically based modeling systems, accounting as they do for a myriad of physical interactions in the three-dimensional domain, can resolve some of the ambiguities inherent in statistical prediction techniques.

Regional climate models (RCMs) use high-resolution horizontal grids and they can, therefore, simulate finer structures of circulation and precipitation distributions than the coarser resolved global models from which seasonal climate outlooks are more commonly sought. The time evolution of planetary-scale climate patterns forced by SSTA can be communicated to a nested regional model as synchronous lateral boundary conditions (LBCs). Studies show that supplying such boundary conditions allows a reasonably accurate simulation of the local climate (Giorgi and Marinucci 1996; Giorgi and Mearns 1999; Fulakeza et al. 2002). Regional model simulations are more than an interpolation of the lower-

Corresponding author address: Dr. Leonard M. Druyan, Center for Climate Systems Research, NASA Goddard Institute for Space Studies, 2880 Broadway, New York, NY 10025.
E-mail: ld12@columbia.edu

resolution data from which the LBC are taken. Downscaling to the finer grid exploits the 4D dynamics of the model, which account for the interaction of mesoscale circulations with a high-resolution representation of local topography. It also attempts to delineate precipitation patterns based on the evolving meteorology.

Most published experiments with dynamic downscaling relate to extratropical regions where the main agents of climate variability are synoptic systems that pass through regional models' lateral boundaries. Some results from the Project to Intercompare Regional Climate Simulations (PIRCS; Takle et al. 1999) have highlighted the difficulty in modeling regional precipitation even when circulation patterns are skillfully downscaled (Gutowski et al. 2000).

Climatological peak seasonal rainfall over Nordeste and the northern Amazon basin occurs during March–May. Dry years feature anomalous warm March–April SSTA in the tropical North Atlantic and cold SSTA south of the equator (Hastenrath and Heller 1977). During such drought periods, near-surface northeasterly circulation from the North Atlantic is weakened and the main areas of moist convection remain north of Nordeste. Correlations between monthly Nordeste precipitation and Atlantic SST are strongest in April and May, with positive correlations relative to the North Atlantic and negative correlations relative to the South Atlantic (Uvo et al. 1998). Marengo (1992) suggested that accelerated northeasterly trade winds during rainier episodes in northern Amazonia are responsible for enhanced moisture transport from the tropical North Atlantic Ocean into the Amazon basin.

Saulo et al. (2000) used Eta Model forecasts at 40-km grid spacing to document many characteristics of the South American low-level jet, including its role as a conduit of moisture from the Amazon basin to the Del Plata basin. Nobre et al. (2001) have more recently reported a two-tier nesting dynamical downscaling experiment using the National Centers for Environmental Prediction (NCEP) Regional Spectral Model (RSM) over northeast Brazil. Their experimental single 4-month forecast on an 80-km grid improved the time–space variations of precipitation compared to results from the global model, although the 20-km solution was less realistic.

The current study examines the skill of seasonal climate predictions over Brazil by an RCM run on a grid with 50-km spacing. Just as deterministic models now operationally produce credible daily weather forecasts, regional climate models nested within GCMs should be tested for their potential to predict seasonal regional climates for targets of opportunity such as Brazil. The paper documents the performance of projections of March–May seasonal and monthly mean regional climates over northern South America for two contrasting years by the National Aeronautics and Space Administration (NASA) Goddard Institute for Space Studies/Center for Climate Systems Research (GISS/CCSR) RCM when the broadscale climate forcing is supplied from GISS GCM seasonal predictions.

Section 2 describes the models and the simulation experiments that use both predicted and observed SST (section 2c) during two different seasons and observed versus model generated lateral boundary conditions (section 2d). Section 3 discusses the results for precipitation (section 3b), OLR (section 3c), and temperature (section 3d). Conclusions are summarized in section 4.

2. The models and the design of experiments

a. The GISS/CCSR RCM

The RCM at GISS/CCSR uses a Cartesian grid with 50-km spacing for dynamics and incorporates interactive soil moisture. The current version of the RCM was described by Druyan et al. (2000a, 2001) and Fulakeza et al. (2002) for studies over Africa. The RCM solves the primitive equations on 16 sigma surfaces using a semi-Lagrangian advection scheme and semi-implicit time differencing with a time step of 465 s. The treatment of terrestrial and solar radiation transfer includes diurnal and seasonal variations, absorption by greenhouse gases, and interactive clouds. Terrain topography is specified at 50-km resolution, consistent with the horizontal computing grid. Deep convection is parameterized by the Kuo (1974) scheme and modified according to Krishnamurti et al. (1983, 1990).

Soil moisture availability (SMA) is defined as the ratio of soil moisture at the surface to a maximum saturation value (field capacity). The scheme that updates SMA was derived by computing a range of values based on estimates of evaporation (latent heat flux) derived from moisture continuity considerations and estimates of the surface radiative energy balance (see Dastoor and Krishnamurti 1991). These SMA values were subsequently used as the dependent variable in second-order regression against observed 5-day rainfall, albedo, surface temperature, normalized difference vegetation index (NDVI), and terrain relief, from data for southern Africa. The derived second-order regression equation constitutes the RCM's interactive scheme that determines SMA during model simulations. Fulakeza et al. (2002) demonstrate how the regression can be made separately for each of several soil types in order to increase its sensitivity to local ground conditions. In the present study a single function developed and tested on data for southern Africa is used for all land grid elements. In addition, this study relies on multiyear mean values of NDVI, although the potential exists to substitute satellite radiometric observations in future experiments. Land surface albedo evolves during the simulation according to variations in SMA, following Deardoff (1978). In summary, the RCM computes SMA interactively as a function of model rainfall, albedo, and surface temperature, as well as observed NDVI. The scheme does not require a long spinup to charge the

TABLE 1. The design of the simulation experiments.

Experiment	No. of runs	Period	SST	LBCs
PRED	5	MAM 1985	Persistance of Feb 1985 SSTA	GISS GCM prediction
	5	MAM 1997	Persistance of Feb 1997 SSTA	GISS GCM prediction
PREDc	5	MAM 1997	Observed 1997 SST	GISS GCM prediction
DNR	5	MAM 1985	Observed 1985 SST	NCEP reanalysis
	5	MAM 1997	Observed 1997 SST	NCEP reanalysis

ground water reservoir, but rather creates evolving SMA distributions early in the simulations that remain fully compatible with the model's local precipitation and temperature history. Fulakeza et al. (2002) showed that RCM-predicted soil moisture and albedo have an impact on simulated rainfall over southern Africa through the modification of sensible and latent heat fluxes.

Prescribed LBCs force the predicted RCM evolution by weighting them with progressively decreasing weights inward within a six-grid buffer zone that completely surrounds the domain of interest.

b. The GISS GCM

The GISS GCM, which provides LBCs for the seasonal prediction experiments, has been extensively used in climate sensitivity studies (e.g., Hansen et al. 1997). A recent description is given by Druyan et al. (2000b), but the vertical resolution has since been increased from 9 to 12 levels while the standard horizontal grid resolution is 4° by 5°. The model employs the land surface scheme of Rosenzweig and Abramopolous (1997), convection and cloud liquid water schemes by Del Genio et al. (1996), and boundary layer physics by Hartke and Rind (1997). Rind and Lerner (1996) discuss the influence of these components on the quality of simulations.

c. The SST projection

The study evaluates the results of climate prediction experiments with the RCM for two 3-month periods, March–April–May 1985 (MAM85) and 1997 (MAM97; see Table 1). In all, 10 simulations were made for MAM85 and 15 for MAM97. Fifteen seasonal predictions were driven by LBCs from corresponding GCM simulations. The basic approach was to initialize the GISS GCM with an arbitrary model dataset for 24 February and run each simulation through 30 May, using SST formed by the persistence of February SSTA superimposed on the climatology. However, Giorgi and Bi (2000) caution that the internal variability of regional model simulations can be important in climates dominated by local convection and land–atmosphere interactions. Therefore, parallel RCM simulations were forced with an additional four sets of LBCs for each year, created from GCM runs with initial conditions that were perturbed by adding random numbers to the initial temperature fields. LBCs from the five GCM simulations were used to force five corresponding RCM simulations that were initialized with NCEP reanalysis datasets (at 0000 UTC) on each of five days, 20–24 February, respectively. The resulting five RCM simulations for each season were averaged to create ensemble seasonal climate predictions (hereafter PRED) that are analyzed below.

Section 1 discussed the causal influences of SST on the evolution of the northern Brazil (austral) autumnal climate. Predicted SSTA in the tropical Atlantic and Pacific are a crucial part of the forcing that determines the outcome of MAM climate predictions considered here. We have assumed that persistence is a reasonable approach for obtaining useful forecasts of SST for the designed 3-month range of the projections. SST formed by persisting initial anomalies, of course, incorporates the climatological seasonal cycle. For both years of the study, SSTA were computed for February from datasets based on Reynolds and Smith (1994) and added, in turn, to the multiyear monthly mean SST of March, April, and May in order to specify the ''predicted'' fields. The GCM automatically interpolates these prescribed monthly mean SST to daily values by fitting them to a sine function.

Figures 1a,b show the SSTA distribution for February 1985 (relative to 1950–85) and February 1997 (relative to 1950–97) over the oceans adjacent to South America between 30°N and 30°S. Negative values over the equatorial Pacific in Fig. 1a identify the waning stages of a cold ENSO event that began during 1984. In addition, a dipole of SSTA is evident in the Atlantic Ocean, negative SSTA north of the equator opposite positive SSTA to the south, the classic pattern for enhancement of Nordeste precipitation during austral autumn (discussed above). The reverse dipole of Atlantic SSTA for February 1997 (Fig. 1b) is more consistent with drought conditions in Nordeste (see above).

Figure 2 shows the distributions of SSTA errors that resulted from the persistence forecasts for each monthly mean during MAM85 and MAM97. During MAM85, most errors are within ± 1.0, but larger errors begin to appear over more extensive areas by May. The errors do not significantly affect the meridional gradient of SST in the western tropical Atlantic to which the ITCZ position over Brazil is sensitive. However, large negative errors in the Atlantic south of 20°S during April–May 1985, imply that February negative SSTA in this region did not, in fact, persist as assumed. MAM97 marked a transition into an ENSO warm phase. Figures 2e,f show that persistence SST forecasts based on Feb-

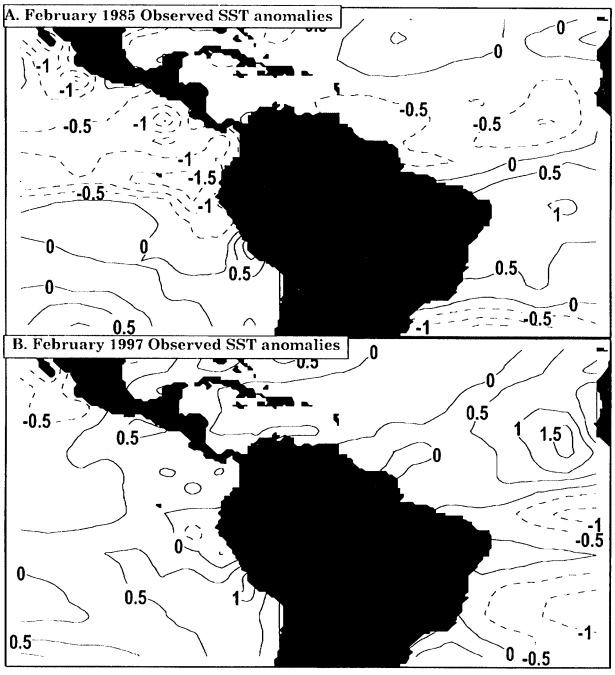

FIG. 1. SSTAs (K), adjacent to South America between 30°N and 30°S: (a) Feb 1985 (relative to 1950–85), (b) Feb 1997, (relative to 1950–97).

ruary 1997 SSTA were as much as 3.5°C too cold in the equatorial Pacific compared to the swath of elevated SST observed during the developing El Niño. SST errors in the western Atlantic were smaller, although negative errors near 20°S are noted, especially in May 1997.

d. The relative influences of lateral and lower boundary conditions

To what extent are the regional seasonal climate predictions compromised by errors in SST predictions? To address this question, the study also evaluates a five-run ensemble of PRED control simulations for MAM97 that used *observed* SST in place of the persistence predictions. The resulting product represents climate predictions from a ''perfect'' forecast of future SST. Results of this ensemble (hereafter PREDc) provide a measure of the sensitivity of the modeling system to the quality of SST predictions.

To what extent were the regional seasonal climate predictions compromised by errors in the predicted circulation, temperature, and humidity provided at the lateral boundaries? Parallel to the RCM predictions discussed above for each of the two seasons, ensembles of five 3-month simulations of RCM-downscaled NCEP reanalysis fields (hereafter DNR) were completed to serve as an additional control for the climate predictions and to be evaluated as a representation of the local climate. Each simulation was begun from one of five different NCEP reanalysis datasets, 20–24 February 1997, as in the seasonal predictions. LBCs for the DNR were interpolated from four times daily synchronous NCEP reanalysis data (Kistler et al. 2001), which include observed SST. Differences between mean model fields of the five runs are a measure of the internal variability of the RCM and/or a measure of sensitivity to initial conditions. Differences between the ensemble seasonal climate predictions (PRED) and the corresponding DNR ensemble show the impact of using ''observed'' versus predicted boundary conditions (LBCs and SST).

NCEP reanalysis climate fields represent an assimilation of raw meteorological observations into an evolving global simulation. Over data-sparse regions the reanalysis is considerably influenced by the characteristics of the NCEP GCM (Kistler et al. 2001). For many climate fields the NCEP reanalysis is a useful representation of the actual atmospheric state, although less so for the precipitation distribution. DNR represent a downscaling of reanalysis fields to a higher spatial resolution, achieved by exploiting the RCM's capability to resolve high gradients and local terrain. Shortcomings in DNR may derive from limitations in the RCM's parameterizations of physical processes and/or from imperfect LBCs because of too few assimilated observations. It is also possible that incompatibilities between the NCEP model and the RCM and the nesting method could lead to other degradations in the climate fields. Ideally it might be desirable to represent the local climate by assimilating available raw observations within an RCM integration that is forced by LBCs from NCEP reanalysis data and observed SST at the lower boundary, but producing analyses based on station observations was beyond the scope of the present work.

Precipitation predictions were validated against station rain gauge data (for MAM 1997) as well as against Climate Prediction Center (CPC) Merged Analysis of Precipitation (CMAP) distributions (for both MAM97 and MAM85) that are based on a blend of rain gauge and satellite data gridded at 2.5° (Xie and Arkin 1997). Note, however, that while CMAP distributions are usually a good representation of actual rainfall patterns, they are spatially smoothed estimates and may occasionally be compromised by too little input from rain gauges (Adler et al. 2001).

Table 1 summarizes the design of the 25 simulations analyzed for this study.

3. Results

a. Precipitation rates

Modeled precipitation rates are secondary variables that depend on ambient moisture and thermal stability. Since moist convection onset is triggered by exceeding threshold values, small differences in the primary model variables can give rise to large differences in precipitation rates.

During austral fall, the retreating overhead sun draws areas of maximum precipitation northward over South

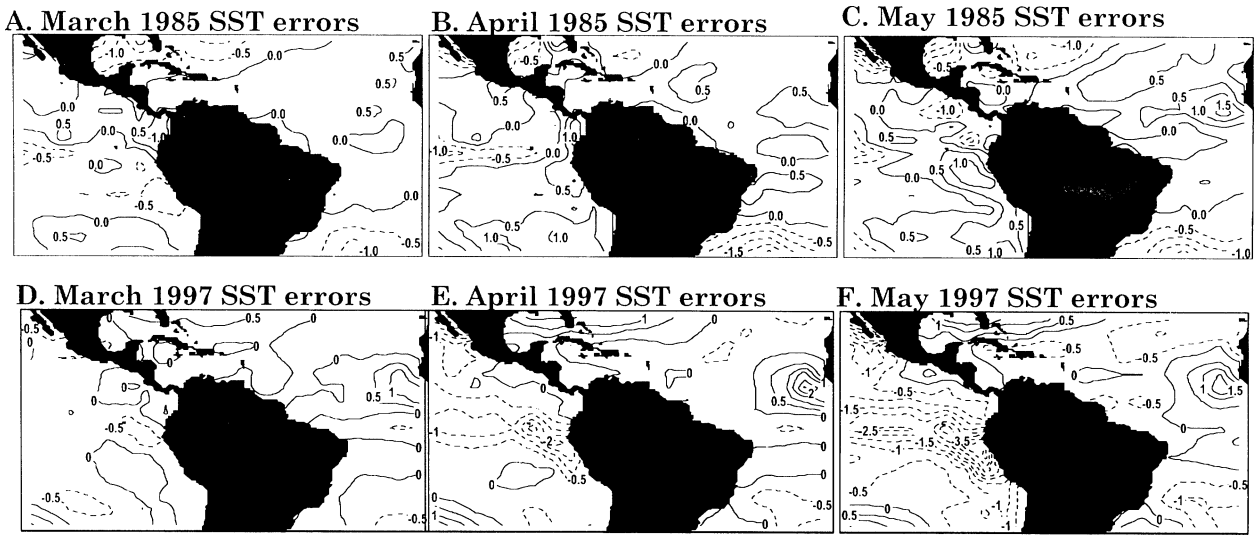

FIG. 2. Errors in monthly mean SST predictions (K) made by persisting Feb SSTA: (a) Mar 1985, (b) Apr 1985, (c) May 1985, (d) Mar 1997, (e) Apr 1997, (f) May 1997.

America. March is marked by heavy rainfall over central Brazil, but by May the maxima cross to the northern side of the Amazon River. Monthly mean distributions of precipitation rates simulated by the RCM DNR and PRED follow this general trend (not shown), but significant differences with CMAP are evident. Consideration of RCM climate predictions for two contrasting seasons offers a glimpse of the model's interannual variability. In association with one of the strongest El Niño episodes of the century during the austral fall of 1997, the northern end of northeast Brazil (Nordeste) experienced anomalously dry conditions, creating extreme shortfalls in crop harvests, and fomenting political unrest (Ropelewski 1999). During MAM85 the ITCZ rainfall maximum was 4°–5° south of its 1997 position over the western Atlantic Ocean and along the coast of northeast Brazil, so MAM97 precipitation totals were up to 9 mm day^{-1} lower for this area (see Figs. 3j–l). The opposite appears to apply to the Amazon basin, however, where MAM97 was up to 3 mm day^{-1} rainier than MAM85, contiguous with rainier conditions along a northwest–southeast swath intersecting the Brazil coast at about 13°S.

1) DNR MAM MEANS

Figure 3 compares the spatial distribution of RCM DNR mean MAM85 and MAM97 precipitation rates (Figs. 3a,b) to CMAP analyses (Figs. 3j,k). The simulated precipitation fields show realistic ITCZ maxima although the boundary forcing does seem to truncate the maxima near the east and west domain boundaries. For MAM97 the DNR ITCZ maximum (Fig. 3a) is too far north over northern Brazil and simulated rates are slightly deficient over northeast Brazil. For MAM 1985 (Fig. 3b) the ITCZ maximum along the northeast coast is correctly enhanced and correctly displaced southward of its MAM97 position. However, DNR MAM85 precipitation rates are too high over central and west Brazil but not high enough over the southernmost Brazilian state. Comparison of Figs. 3c and 3l shows that the DNR succeeded in capturing the MAM97 relative precipitation deficit over northeast Brazil in juxtaposition to the excess north of the equator. While DNR interannual differences correctly depict parts of the western and northern Amazon basin to be rainier in MAM97, they do not reflect the MAM97 excesses within a northwest–southeast swath over central Brazil. Similarly, DNR MAM 1997 minus 1985 positive precipitation differences run contrary to observational evidence over the Atlantic coast near 25°S.

2) PRED MAM MEANS

Figures 3d,e show PRED spatial distributions of MAM97 and MAM85 precipitation rates, and Fig. 3f, the interannual differences. Differences between DNR and PRED result from the different data used for LBCs and/or from using persistence forecasts versus observed SST, but common errors could reflect RCM biases. PRED underestimated MAM97 precipitation rates (Fig. 3d) over northeast Brazil by a greater margin than DNR, but was rainier than both DNR and CMAP over the central and western Amazon basin. PRED was also too dry where the ITCZ crosses the Brazil coast.

Figure 4 shows the MAM97 precipitation distribution for the PREDc ensemble, based on observed SST supplied to both the GCM and the RCM simulations. It is clear that using observed SST did not correct the precipitation deficits simulated by PRED over eastern Brazil. One can deduce that DNR improvements (cf. PRED) over eastern Brazil do not result from using actual SST

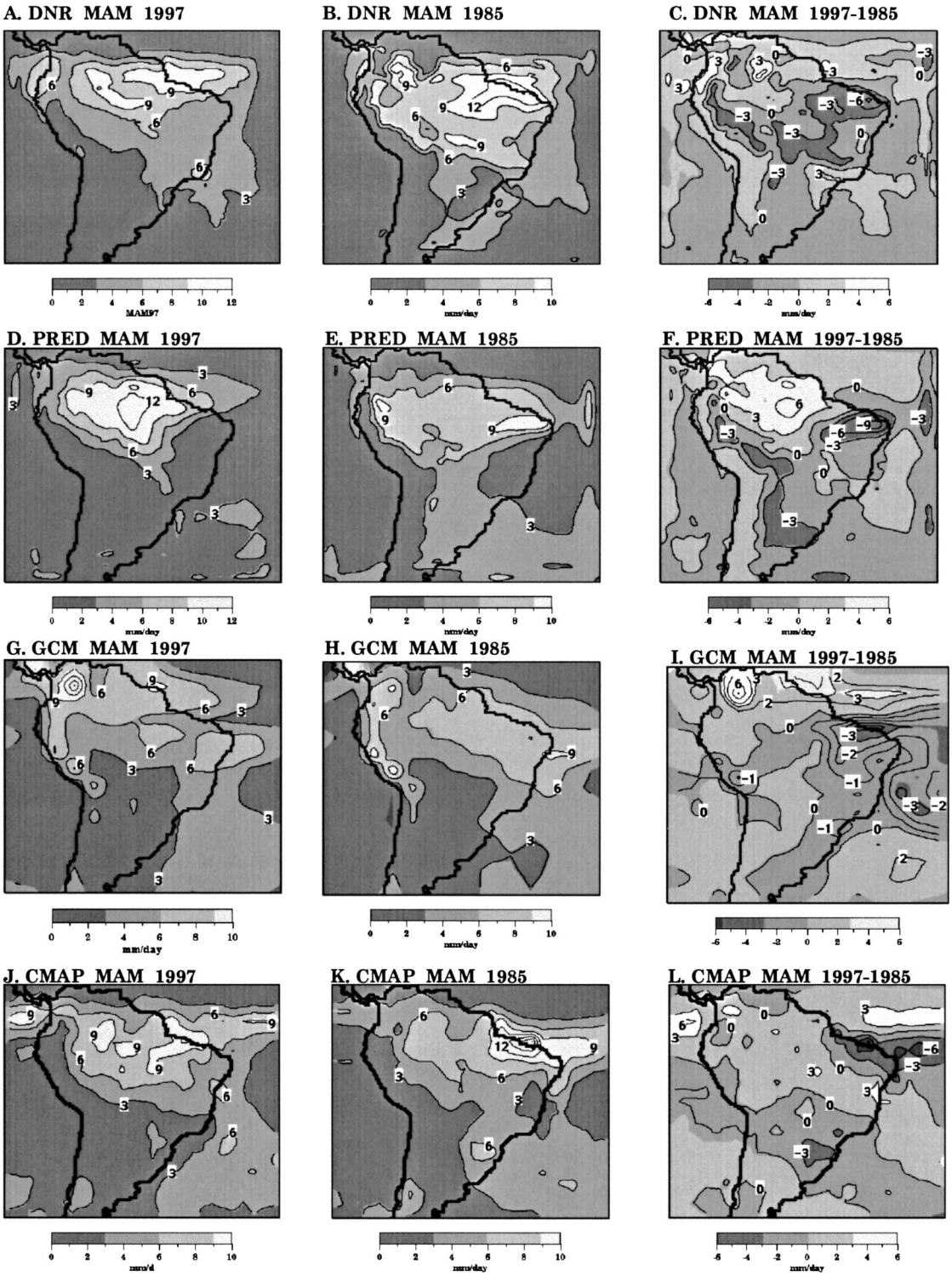

FIG. 3. MAM mean precipitation rates (mm day^{-1}). Note that the graphics software performs a smooth interpolation so that the differing resolution of RCM and GCM fields is somewhat obscured. (a) RCM DNR, MAM 1997; (b) RCM DNR, MAM 1985; (c) RCM DNR, MAM 1997 minus MAM 1985; (d) RCM PRED, MAM 1997; (e) RCM PRED, MAM 1985; (f) RCM PRED, MAM 1997 minus MAM 1985; (g) GCM PRED, MAM 1997; (h) GCM PRED, MAM 1985; (i) GCM PRED, MAM 1997 minus MAM 1985; (j) CMAP (observed), MAM 1997; (k) CMAP (observed), MAM 1985; (l) CMAP (observed), MAM 1997 minus MAM 1985.

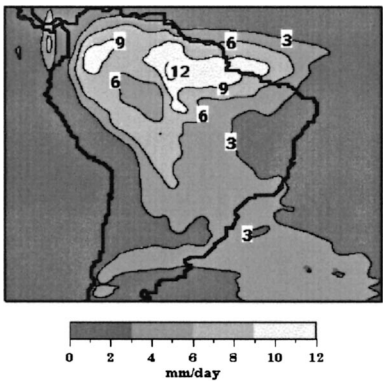

FIG. 4. MAM 1997 mean precipitation rates (mm day^{-1}) for the PREDc ensemble.

lower boundary data, but rather from the benefits of more realistic moisture and circulation fields communicated via LBCs. PREDc precipitation maxima over the Amazon are somewhat more realistic than for PRED (Fig. 3d), and the eastward extension of the ITCZ maximum near the mouth of the Amazon validates better against CMAP. A similar improvement over the eastern Amazon occurred in the GCM results forced by observed SST (not shown).

PRED for MAM85 (Fig. 3e) displaced the ITCZ maximum to the southeast, leading to realistic PRED MAM97 relative deficits along the Brazil northeastern coastline (Fig. 3f). Over the western Amazon, PRED MAM97 relative excesses, although exaggerated, covered a more extensive contiguous area than for DNR, and therefore were a better qualitative match to the CMAP difference field (Fig. 3l).

The influence of resolution on precipitation simulations can be appreciated by comparing PRED to the GCM results (at 4° by 5° grid spacing) in Fig. 3. In addition to resolution effects, PRED/GCM differences can result from the models' different parameterizations and from the nesting procedures. The ensemble mean results for the GISS GCM also show a southeast displacement of the heaviest MAM rainfall from 1997 to 1985, although precipitation rates considerably underestimate CMAP evidence (Figs. 3g,h versus Figs. 3j,k). Moreover, the MAM97 ITCZ is too far north and the southeast displacement of the ITCZ in MAM85 was exaggerated (Fig. 3h), probably in response to positive errors in predicted SST east of Brazil (Fig. 2), making eastern Brazil too rainy in MAM85. Note that the RCM, even when forced by GCM data (PRED and PREDc), provides a more realistic simulation of the ITCZ latitude than the GCM. This emphasizes the complex relationship between RCM fields and LBC forcing. Despite these discrepancies and the coarse resolution, the GCM MAM 1997 minus 1985 differences (Fig. 3i) indicate a very realistic dipole of negative values along the northeast coast in juxtaposition to the positive area along 6°N. Elsewhere, interannual differences in the GCM fields (Fig. 3i) do not correspond to CMAP (Fig. 3l). For example, in a similar vein to the RCM results, MAM97 GCM precipitation deficits were spread southward beyond the observed wedge over northeast Brazil.

RCM-simulated precipitation rates were interpolated to the 2.5° grid lattice and corresponding CMAP fields for MAM97 and MAM85 were subtracted to form ''error'' distributions. Figure 5 compares the resulting spatial distributions of ''errors'' for the DNR and PRED ensembles. Comparison of Figs. 5a and 5b suggests that the DNR precipitation field for MAM 1997 was closer to the observational evidence than PRED. However, the PRED precipitation distribution for MAM 1985 (Fig. 5d) incurred lower errors over most of Brazil than the DNR results for that season. Figure 5 does not show any obvious systematic errors that are common to the four sets of simulations and that might identify areas of RCM bias.

3) RAIN GAUGE DATA

Better spatial detail of the observed precipitation distribution over northeast Brazil is shown from the analysis of rain gauge data that was available for the MAM97 season. Figure 6 shows a meridional cross section of MAM97 precipitation rates averaged over 38°–42°W in northeast Brazil on which DNR and PRED results are compared with rain gauge observations. Note that even seasonal mean rates from neighboring rain gauges often reflect very high spatial variability. Accordingly, the latitudinal profiles in Fig. 6 have also been represented by fitting a smooth curve to rain gauge observations. The cross section shows that both RCM simulation ensembles underestimated precipitation rates between 10° and 16°S, but DNR are somewhat closer to observations in magnitude.

b. Quantitative validation of precipitation

RCM-simulated precipitation rates that were interpolated to the 2.5° grid lattice were also validated as area averages against CMAP values over each of three regions (see Fig. 7): Amazon, 7.5°N–12.5°S, 68°–43°W; northeast Brazil, 2.5°–12.5°S, 40.5°–33.5°W; south Brazil, 15°–30°S, 60.5°–43°W. Tables 2 and 3 give the values of three validation parameters for monthly mean DNR and PRED simulations. Comparison of area-averaged precipitation rates considers whether simulated rainfall rates were comparable to CMAP in a general sense. The rms errors quantify the discrepancies between simulated and observed rainfall at matching grid points, while correlation coefficients indicate how closely the spatial patterns of the simulated rates within each area resemble the patterns in the corresponding CMAP analysis. Correlation coefficients for northeast Brazil have only marginal importance since they refer to a rather small area with only 20 grid elements.

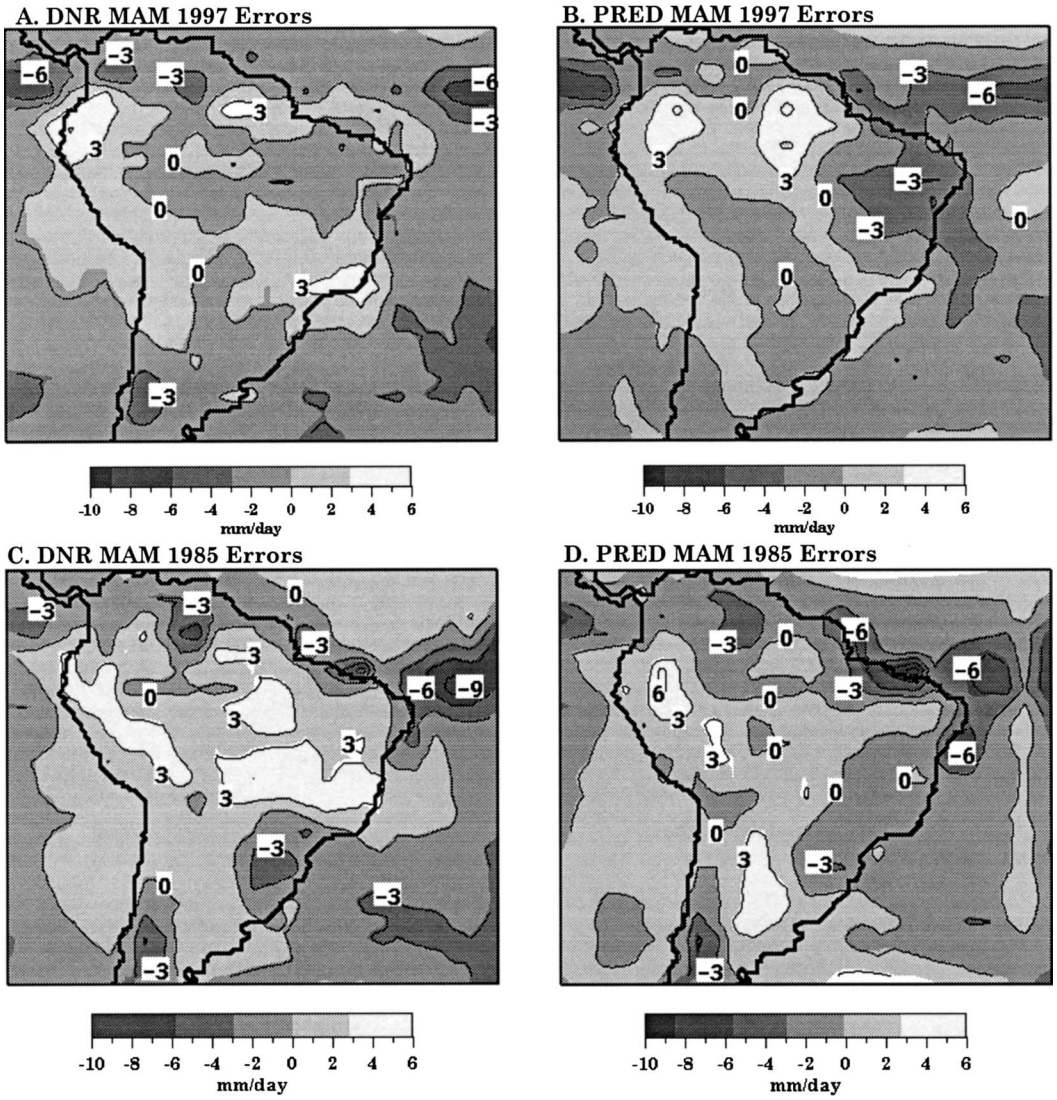

FIG. 5. Differences between simulated and CMAP (observed) precipitation rates (mm day^{-1}): (a) DNR MAM 1997, (b) PRED MAM 1997, (c) DNR MAM 1985, (d) PRED MAM 1985.

1) AREA AVERAGES (TABLE 2)

Results are rather mixed. Modeled area-averaged precipitation rates are close to CMAP values for both the DNR and PRED ensembles in 1997 and 1985 over the south Brazil region, but over the Amazon the 1997 averages validate better than in 1985. The DNR averages over northeast (NE) Brazil are closer to CMAP than PRED in both years, and combined with results from PREDc (Fig. 4) this implies that GCM LBC errors are more likely the cause of poor RCM performance than imperfect SST predictions.

Systematic simulation errors can be eliminated by considering the 1997 minus 1985 differences in Table 2. Trends of the monthly 1997 minus 1985 differences in area-averaged precipitation rates are somewhat parallel with CMAP only for PRED over the Amazon and DNR over NE Brazil.

2) THE RMS ERRORS AND CORRELATION COEFFICIENTS (TABLE 3)

(i) Amazon

Correlation coefficients (R) between spatial distributions of DNR and CMAP monthly precipitation and between PRED and CMAP monthly precipitation over the Amazon area are significant with better than 95% confidence. DNR scores better in MAM97 ($0.63 < R < 0.72$) and PRED better in MAM 1985 ($0.47 < R < 0.79$). Corresponding rms errors are mostly between 40% and 80% of the area-average precipitation rates.

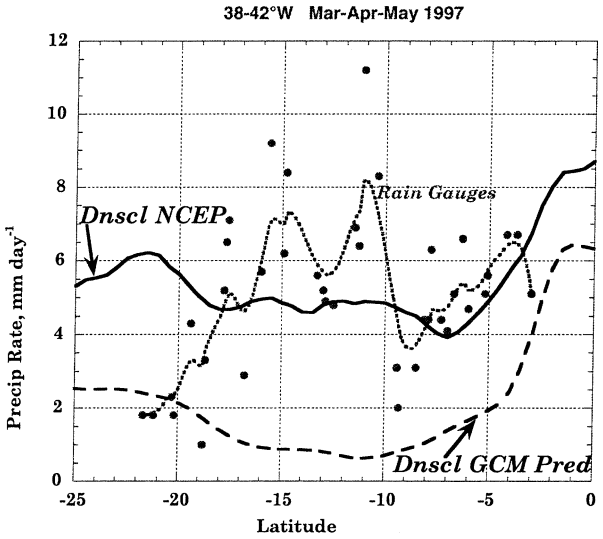

FIG. 6. MAM 1997 precipitation rates (mm day^{-1}) vs lat within the swath 0°–25°S, 38°–42°W. Solid line: RCM DNR; dashed line: PRED; dots: rain gauge observations; dotted line: smooth fit to rain gauge observations.

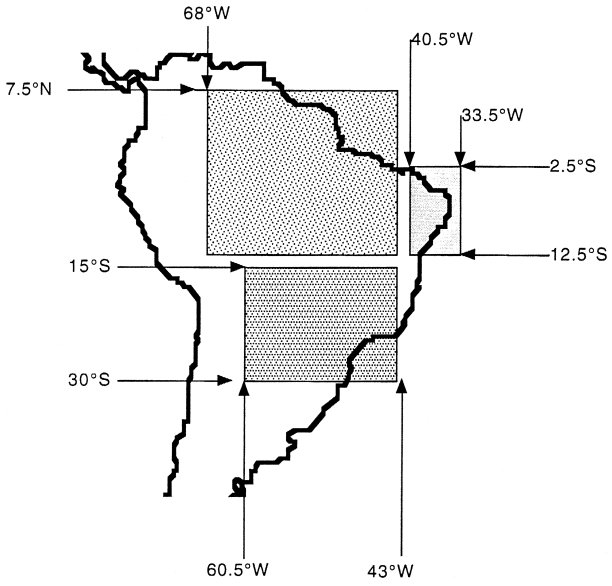

FIG. 7. Three regions for the validation of RCM precipitation: Amazon, bounded by 7.5°N–12.5°S, 68°–43°W; Nordeste, bounded by 2.5°–12.5°S, 40.5°–33.5°W; South Brazil, bounded by 15°–30°S, 60.5°–43°W.

Both the rms and the correlation coefficient trends imply a slight improvement of the simulated precipitation distributions over the Amazon with elapsed time. The May 1985 and 1997 PRED patterns validated especially well with CMAP, with low rms error, high R, and almost the same area average. March PRED for both years underforecast precipitation rates over the Amazon region, achieving only 0.45–0.47 correlation coefficients with their corresponding CMAP fields.

(ii) South Brazil

The rather low area-average rainfall rates for MAM97 are matched fairly well by both DNR and PRED and their rms errors are correspondingly low (Table 3). Except for DNR in March 1997 and PRED in May 1985, spatial distributions of modeled rainfall over south Brazil were not significantly correlated with CMAP. (The $R > 0.26$ are significant at the 95% confidence level.) The simulations of low area-average rainfall for April 1997 are realistic, but there is no spatial correlation with the corresponding CMAP pattern.

According to CMAP data, south Brazil was rainier in MAM 1985 than in the corresponding 1997 period. The RCM reproduced the relative deficits, although the isohyetal spatial patterns were not well correlated and rms errors were rather high.

(iii) NE Brazil

The R are also shown in Table 3, although they are of questionable diagnostic value over this small area of only 20 grid elements. (The $R > 0.43$ are significant at the 95% confidence level.) In most respects, DNR gave a better representation of the observed precipitation regime over NE Brazil than PRED. Realistic area averages were noted for the DNR ensemble for all months and

TABLE 2. Area-average monthly precipitation rates (mm day^{-1}) for RCM experiments ensembles, PRED and DNR (see text), vs CMAP values. Regions are defined in Fig. 7.

	Amazon			South Brazil			Northeast Brazil		
Region	PRED	DNR	CMAP	PRED	DNR	CMAP	PRED	DNR	CMAP
Mar 1985	5.7	8.6	7.2	4.8	5.1	4.8	6.1	7.5	7.0
Apr 1985	4.8	9.6	6.4	3.3	3.1	4.5	5.6	10.4	11.2
May 1985	6.9	4.4	6.5	3.2	5.0	2.1	2.1	3.8	5.2
Mar 1997	8.0	7.3	9.2	2.2	4.0	3.1	1.1	5.3	8.6
Apr 1997	6.7	6.8	6.8	2.5	2.2	2.2	1.8	5.0	4.7
May 1997	7.0	6.4	6.0	1.5	3.2	2.3	1.9	3.7	2.9
Δ1997–85									
Mar	2.3	−1.3	2.0	−2.6	−1.1	−1.7	−5.0	−2.2	−1.6
Apr	1.9	−2.8	0.4	−0.8	−0.9	−2.3	−3.8	−5.4	−6.5
May	0.1	2.0	−0.5	−1.7	−1.8	−0.2	−0.2	−0.1	−2.3

TABLE 3. The rms errors (mm day^{-1}) and correlation coefficients (cc) between monthly mean precipitation arrays for the selected regions (defined in Fig. 7) vs corresponding CMAP distributions. Correlations significant at the 95% confidence level are in boldface.

	Amazon		South Brazil		Northeast Brazil	
Region	PRED	DNR	PRED	DNR	PRED	DNR
	Rms errors					
Mar 1985	4.1	5.5	2.9	6.5	3.2	3.9
Apr 1985	3.8	5.6	2.8	3.4	8.1	5.7
May 1985	2.9	4.4	2.0	3.7	3.6	3.6
Mar 1997	5.2	3.6	2.5	2.3	8.2	4.7
Apr 1997	2.8	2.7	1.2	2.0	3.2	1.8
May 1997	3.4	3.1	1.7	2.3	2.3	2.0
	Correlation coefficients					
Mar 1985	**0.47**	**0.38**	−0.36	**0.26**	**0.79**	**0.66**
Apr 1985	**0.50**	**0.44**	−0.18	−0.41	0.30	−0.07
May 1985	**0.78**	**0.49**	**0.44**	0.18	**0.62**	**0.58**
Mar 1997	**0.45**	**0.72**	0.16	**0.54**	0.19	0.28
Apr 1997	**0.60**	**0.72**	0.19	0.17	**0.61**	**0.47**
May 1997	**0.67**	**0.63**	0.09	0.23	−0.07	0.42

the spatial patterns were significantly correlated with CMAP in April 1997 and March and May 1985. The rms precipitation rate errors for DNR were some 40%–60% of area averages for four of the six months, otherwise they were higher.

This region experienced an increase in average precipitation rates from March to April 1985, followed by a decrease in May. This trend in area-average precipitation rates was captured by DNR, although the corresponding spatial distributions of precipitation were correlated with CMAP only for March ($R = 0.65$) and May ($R = 0.59$). The DNR rms error for these months is about 55% of area-averaged precipitation. Although the PRED results for MAM 1985 underestimated area-average precipitation rates for NE Brazil, incurring rather large rms errors, PRED R values were statistically significant and higher than for DNR for both March and May 1985. Nobre et al. (2001) found rms errors of mostly 3–4 mm day^{-1} between their RSM (at 80 km) monthly precipitation predictions for January–April 1999 and rain gauge measurements over NE Brazil. Table 3 shows that both the DNR and PRED ensembles achieve rms errors smaller than 4 mm day^{-1} over this region for four of the six months.

In summary, the quantitative validation of simulated monthly precipitation rates over three regions showed the following:

1) RCM precipitation simulations for some selected months and regions validate well against CMAP data, but such positive results are not consistently obtained.
2) Predicted fields (PRED) were not consistently worse than the downscaled reanalysis (DNR).
3) There is no strong evidence that either simulation improves or deteriorates with elapsed time during the season.
4) Spatial patterns of monthly RCM mean precipitation over the Amazon were consistently correlated with corresponding CMAP fields, and MAM 1997 results were better than MAM 1985. Results over the other two regions were less consistent.

3) UNFORCED VARIABILITY OF PRECIPITATION SIMULATIONS

The DNR experiments were forced with NCEP reanalysis data as synchronous lateral boundary conditions. Variability between the five ensemble members was introduced by starting each simulation from a different NCEP reanalysis initial condition, 20–24 February 1997. Average Amazon region precipitation rates are next compared to determine how the variability between runs changes each month as the simulations lengthen. Figure 8a shows the average precipitation rate over the Amazon for each month and for each run. April shows the largest variability (between the runs), perhaps because it is a transition month during which the focus of heavy precipitation is moving northward through the Amazon region. The dispersion of average May values is comparable to the March cluster, so variability between ensemble members is not monotonically increasing. This implies that the boundary data, which is common to all of the runs, has a controlling influence on the results. Figure 8a also shows DNR ensemble mean (Amazon region) values and the corresponding CMAP data. Note that, although the DNR underestimated March precipitation rates, it provided quite realistic estimates for April and May.

Figure 8b shows correlations between DNR precipitation distributions over the Amazon region for each possible pair of runs. The general pattern of increasing correlations from March to May has only a few exceptions. By May, all of the correlations exceed 0.60, and 6 out of 10 exceed 0.90. This reinforces the conclusion that results between ensemble members of the DNR experiment tend to converge with time, probably because they are all driven by the same NCEP reanalysis data.

How does the variability of simulated monthly precipitation fields affect the skill in reproducing the observed distribution? Figure 8c shows correlation coefficients between corresponding gridded arrays for each simulation and CMAP monthly means over the Amazon region. Although only two of the simulations had consistently high correlations with CMAP data for each of the three months, the ensemble mean pattern retains a high correlation for all months. Two of the simulations show rather low correlations in March, but recover somewhat by April. However, run B was very poorly correlated with CMAP also in May. Even though the variability between runs was found to decrease by May, agreement with the observational evidence did not in-

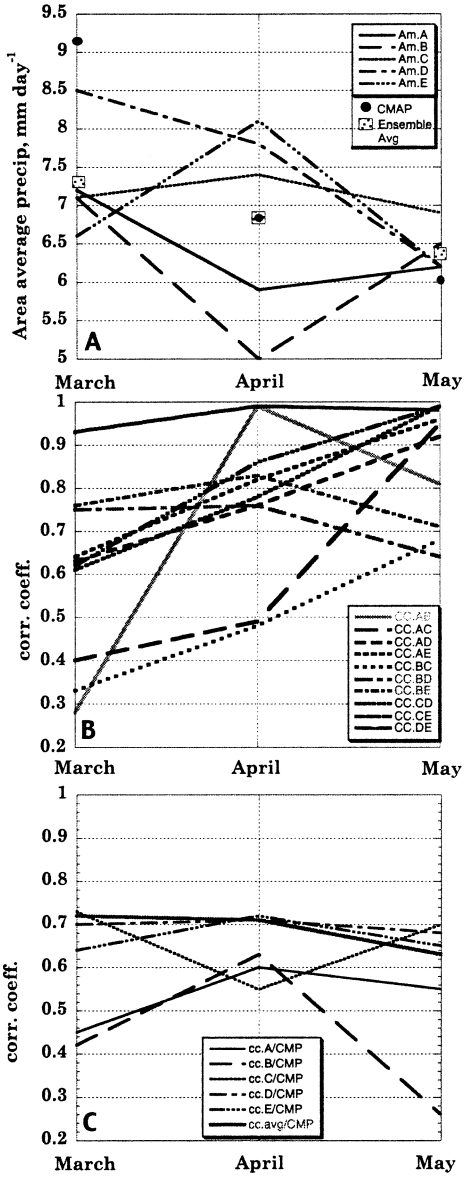

FIG. 8. (a) Amazon region average monthly mean precipitation rates (mm day^{-1}) for each simulation in the DNR ensemble. Corresponding CMAP values are indicated by dots and ensemble means by squares. (b) Correlation coefficients between precipitation rate distributions over the Amazon of all pairs of DNR simulations. (c) Correlation coefficients between precipitation rate distributions over the Amazon of each DNR simulation vs the corresponding CMAP distribution, and between the DNR ensemble average and CMAP (thick gray line).

crease, so May was not more skillfully forecast than March or April.

c. OLR

Outgoing longwave radiation (OLR) has been measured by the National Oceanic and Atmospheric Administration's (NOAA's) satellites for many years (Liebmann and Smith 1996). Cold cloud tops in the Tropics are identified by OLR minima, while OLR maxima imply relatively cloud-free areas. Xie and Arkin (1997) used OLR as a major but not exclusive component in creating CMAP datasets. Liebmann et al. (1998) found that OLR from NCEP reanalyses over the Amazon basin has at best a 0.6 correlation with observed rainfall and a poorer correlation with NCEP reanalysis precipitation fields. These latter are, in turn, not a very realistic representation of actual rainfall patterns.

Since OLR is directly measured by satellite-borne instrumentation, and because of the direct association between OLR and precipitation and clouds, this variable is a valuable diagnostic for validating simulations of climate and weather.

The MAM97 mean OLR for the RCM DNR ensemble (Fig. 9a) can be compared to the observed distribution (Fig. 9c). Simulated OLR are about 10 W m^{-2} too high over eastern Brazil, an indication that observed anomalous convective activity was somewhat underestimated by the DNR simulation. Moreover, the latitude of the DNR ITCZ minimum over the Atlantic is closer to the climatological position than to the 1997 one and model cloud tops were too cold over the entire length of the Amazon. Observed OLR between 250 and 260 W m^{-2} during MAM 1997 over southern Brazil were anomalously high and the RCM DNR represents this feature quite well. The mean MAM97 OLR in Fig. 9b (PRED) are an improvement over the corresponding DNR values (Fig. 9a) over east Brazil, the Amazon, and the ITCZ, although not with respect to the latitude of the ITCZ OLR minimum. Lower PRED OLR along the Atlantic coast at 15°S are evidence of more convective activity.

MAM85 ITCZ minimum OLR (Fig. 9f) were aligned along the northern coast of Brazil, 3°–5°S, indicating a southward displacement of the ITCZ from its MAM97 position. PRED OLR (Fig. 9e) achieves a more realistic ITCZ structure compared to DNR results (Fig. 9d). In particular the gradient of PRED OLR across the northeast corner of Brazil was very close to the observed pattern. Moreover, PRED has better success in reproducing OLR evidence of convective activity near 50°W over southern Brazil. However, both RCM simulations for MAM85 (Figs. 9d,e) do not adequately represent the highest (coldest) cloud tops over the western Amazon, although here too PRED is more realistic.

Observed MAM 1997 minus 1985 OLR differences (ΔOLR; Fig. 9i) emphasize the meridional shift of the ITCZ between these two seasons. The relative northward displacement during 1997 forms a distinct wedge of positive ΔOLR over northeast Brazil in juxtaposition to the swath of negative ΔOLR north of the equator. The DNR (Fig. 9g) also shows this dipole pattern of ΔOLR, but the negative node is along the equator and the positive node is too weak. In addition, the DNR has exaggerated the magnitude of negative ΔOLR over equatorial Brazil, while an observed negative area along the Atlantic coast at 15°S has been barely represented. PRED ΔOLR (Fig. 9h) validates better against the ob-

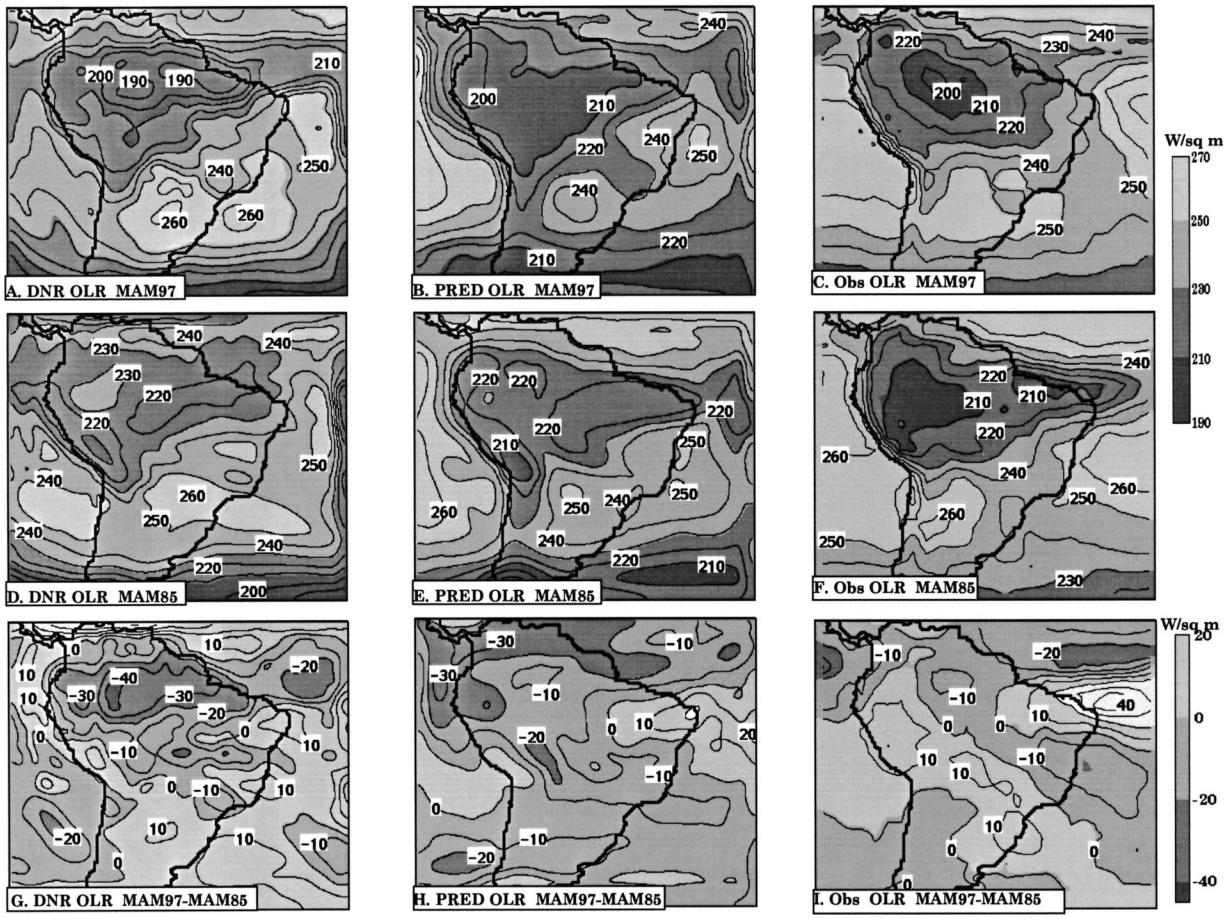

FIG. 9. OLR (W m^{-2}): (a) DNR, MAM 1997; (b) PRED, MAM 1997; (c) observed, MAM 1997; (d) DNR, MAM 1985; (e) PRED, MAM 1985; (f) observed, MAM 1985; (g) DNR, MAM 1997 minus MAM 1985; (h) PRED, MAM 1997 minus MAM 1985; (i) observed, MAM 1997 minus MAM 1985.

servations, although some of the simulation errors are repeated. The most impressive PRED improvement is the stronger and therefore more realistic positive ΔOLR wedge near the northeast corner of Brazil. PRED improvements in the OLR distribution for both seasons have also reproduced the observed northwest–southeast oriented zone of negative ΔOLR along the Atlantic coast at 15°S, although it is slightly displaced southward. Note that the PRED advantages are not as evident for the simulated interannual precipitation differences (Figs. 3c,f,l) which, although related to OLR, nevertheless reflect different aspects of model complexities.

PRED simulations used lower spatial resolution GCM-predicted fields than NCEP data used for the DNR. The foregoing comparison indicates that PRED provided more realistic spatial distributions of seasonal mean OLR than by using NCEP reanalysis data as LBCs, despite the fact that the GCM data were predicted. It is possible that there are some incompatibilities between the NCEP reanalysis boundary conditions and the RCM, whether in the moisture or the circulation data, which have a negative impact on the simulated moist convection.

d. Temperature cross section

1) MAM97

Figure 10a shows north–south cross sections of mean MAM97 potential temperature (θ) along 40°W at three levels for the RCM DNR, PRED, and for NCEP. At 1000 mb, the analyzed maximum θ occurs at 2.5°S, but it slopes southward with altitude, reaching about 5°S at 850 mb. The DNR maximum θ at 1000 mb occurs at 3.5°S, and at 7.5°S at 850 mb. The DNR and PRED are both too warm at 850 mb, implying greater thermal stability than NCEP. DNR and PRED positive θ departures are almost 3 K at 15°S. The PRED simulation ensemble θ for MAM97 are slightly colder at 1000 mb than DNR, probably owing to negative SST prediction errors. PRED θ at 700 mb are cooler than DNR, validating somewhat better against NCEP values south of 10°S. The RCM maintains a positive temperature bias

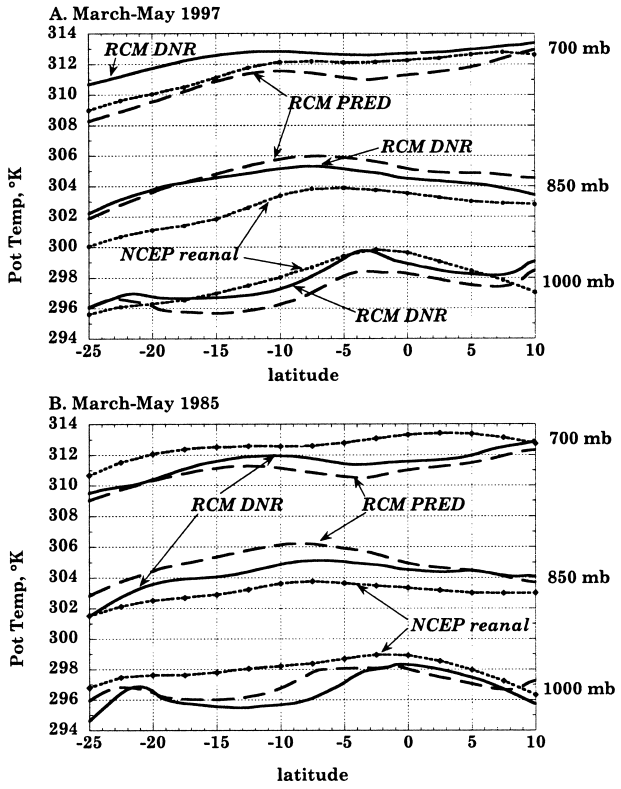

FIG. 10. Latitudinal profiles of potential temperature along 40°W, from 10°N to 25°S: (a) MAM 1997; (b) MAM 1985. Lowermost profiles are at 1000 mb, middle profiles are at 850 mb, and upper profiles at 700 mb.

of about 2 K relative to NCEP at 850 mb over most of tropical South America (not shown). It is apparently not related to surface heating since the modeled temperature is cooler than NCEP near the surface. Reasons for the bias are the focus of current investigation.

2) MAM85

The simulated DNR and PRED profiles of θ along 40°W for MAM85 (Fig. 10b) show biases similar to MAM97. In this case, the cool biases at 1000 mb are larger, while the warm biases at 850 mb are lower. Here too, the simulated thermal structure below 850 mb is more stable than analyzed, but less stable between 850 and 700 mb. The largest simulation errors at 1000 mb are at the latitudes where the cross section is over land, but there is no obvious connection between the errors at each of the three levels. PRED temperature errors at 1000 mb over this interval are smaller than DNR errors, but the reverse is true at 850 and 700 mb.

In summary, the simulated temperature structure along 40°W for both seasons is reasonable, showing the largest discrepancies over the subtropics with maximum excesses at 850 mb during both seasons. While observed interannual θ differences are qualitatively simulated in the Tropics, rather significant departures from NCEP were evident over the subtropics. What seems to be an RCM bias for warm temperatures at 850 mb is for the most part slightly worse in PRED.

e. Meridional wind cross sections

The ITCZ represents a zone of meridional wind (v) convergence in the lower troposphere. Figure 11 shows the mean MAM97 and MAM85 latitude–height cross sections of v for the DNR and PRED ensemble simulations along 40°W, compared to the same fields from NCEP reanalyses. Northerlies north of the equator, which are well developed during the entire austral fall (Figs. 11c,f), are well simulated in the DNR (Figs. 11a,d), including their vertical extent to 850 mb. NCEP moves the confluence of the ITCZ gradually northward from 7°S in March 1997 to 3°S in April to the equator in May (not shown). However, the 2.5° resolution of the NCEP grid makes these latitudes somewhat indefinite, as is the latitude of the MAM97 average confluence at 2.5°S (Fig. 11c). There is almost no intraseasonal migration of the confluence latitude in the corresponding DNR simulation, which moves from the equator in March to 1°N in April and May. In tandem with the southward spread of southerlies in the midtroposphere about which both sets of analyses agree, near-surface southerlies between 5° and 10°S strengthen throughout this period. However, NCEP establishes the core of maximum southerly circulation at 950 mb, evident in the MAM97 cross section, while the DNR confines the strongest southerlies to the near-surface layer. In addition, the DNR transition back to northerlies (13°S) is slightly displaced from the NCEP position (19°S).

Negative v north of the equator are weaker and occupy a shallower layer in the PRED MAM97 results (Fig. 11b). The corresponding ITCZ confluence occurs some 4° farther south than for DNR, which is just as plausible. However, the northerly component of circulation at the southern end of the cross section is apparently too strong in these ensemble results.

Consistent with the relative southward displacement of the ITCZ precipitation maximum and OLR minimum during MAM85, the ITCZ confluence was also south of its MAM97 position (5°S; Fig. 11f). In addition, the northerlies over the North Atlantic were stronger and the southerlies over Nordeste were slightly weaker. The DNR and PRED simulations agree qualitatively with these interannual differences, although PRED southerlies over Nordeste were only marginally different for the two years. Neither the DNR (Fig. 11d) nor PRED (Fig. 11e) develop the deep layer of strong northerlies south of 20°S during MAM85 that is analyzed by NCEP (Fig. 11f).

Both DNR and PRED cross sections indicate stronger v gradients across the ITCZ than NCEP. This is probably a more realistic representation of the circulation, made possible by the higher spatial resolution of the RCM grid.

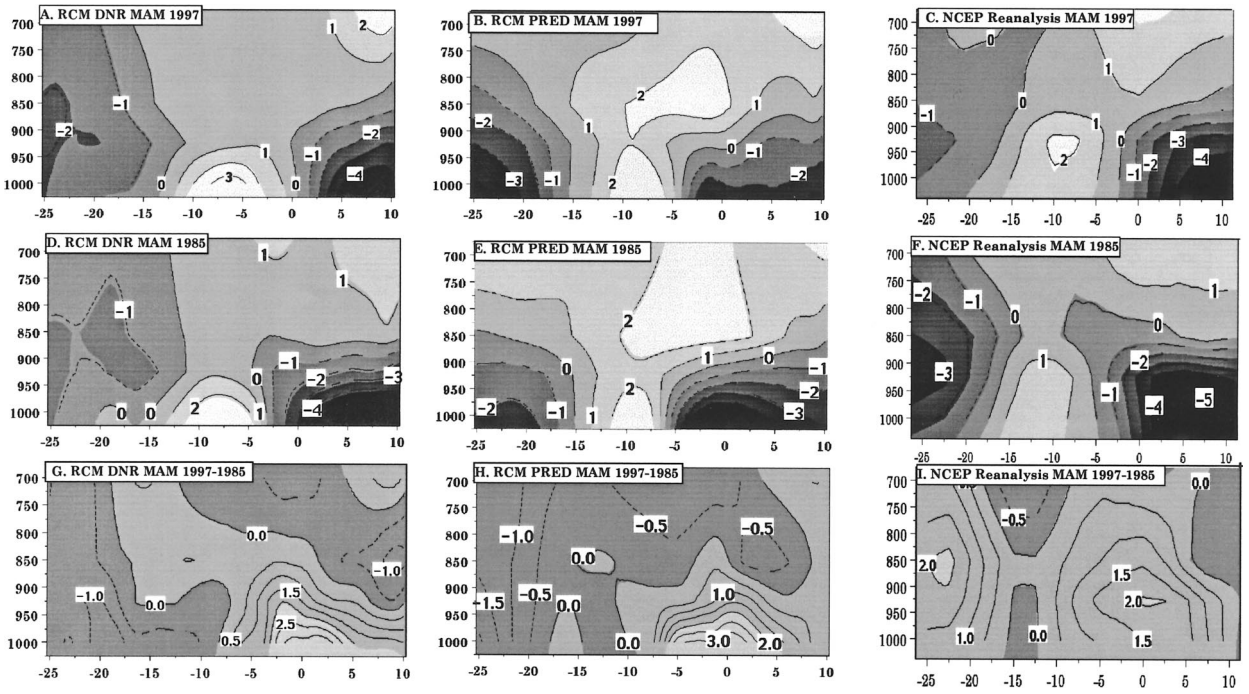

FIG. 11. Latitude–pressure cross sections of the MAM meridional wind component (m s^{-1}): (a) DNR, 1997; (b) PRED, 1997; (c) NCEP, 1997; (d) DNR, 1985; (e) PRED, 1985; (f) NCEP, 1985; (g) DNR, 1997 minus 1985; (h) PRED, 1997 minus 1985; (i) NCEP, 1997 minus 1985.

The analyzed (NCEP) MAM 1997 minus 1985 v differences (Δv) along the same cross section are shown in Fig. 11i. Positive Δv centered at the equator reflect the stronger southerlies of 1997 and the stronger northerlies of 1985. The DNR and PRED ensembles successfully reproduce this pattern although they exaggerate Δv in the lowest level. South of 15°S, the RCM Δv is the wrong sign owing to disagreements with NCEP in the strength of northerlies during both seasons.

4. Conclusions

This study describes the dynamic downscaling of seasonal climate predictions over South America to a 0.5° grid by means of simulations with the GISS/CCSR Regional Climate Model (RCM). Ensembles of five climate predictions for March–May 1985 (1997) were made with the GISS GCM by persisting February 1985 (1997) SST anomalies. The interpolated GCM predicted fields, generated on a 4° latitude by 5° longitude grid, served as synchronous lateral boundary conditions (LBC) for the five RCM PRED simulations initialized with NCEP reanalysis data on each of five days, 20–24 February, 1985 (1997). Parallel control simulation ensembles (DNR) were driven by synchronous NCEP reanalysis data for the same periods. DNR simulations, which used observed SST boundary conditions, provided a standard against which the impact of imperfectly predicted lateral and lower boundary conditions used in PRED were evaluated. A second control ensemble (PREDc) was run like PRED, except that it used observed SST in order to separate the impacts of LBCs from those of imperfect SST predictions.

Results imply that even using actual climate data to drive the RCM does not guarantee realistic modeled precipitation distributions. For example, NCEP reanalysis precipitation distributions often contradict the Climate Prediction Center (CPC) Merged Analysis of Precipitation (CMAP) and rain gauge evidence over tropical South America. It is, therefore, not surprising that RCM downscaled precipitation distributions from the DNR ensemble were not unequivocally more skillful than corresponding PRED results.

MAM85 was rainier in northeast Brazil than MAM97, owing to the southeastward displacement of the ITCZ, and some of these differences were captured by both DNR and PRED ensembles. However, PRED precipitation deficits over most of east Brazil and excesses in the Amazon in MAM97 were more extreme than DNR errors. These PRED discrepancies were not remedied by using observed SST, implying that the adverse outcome was a consequence of the GCM forcing.

GISS GCM projections featured an excessive southeast displacement of the ITCZ in MAM85 that was considerably improved by PRED and PREDc downscaling to the higher resolution. The MAM85 southeastward displacement of the ITCZ was also evident in satellite measurements of outgoing longwave radiation (OLR). ITCZ minimum OLR were slightly underestimated by the RCM and not far enough north over the Atlantic in

MAM97. The PRED ensemble achieved a slightly more realistic northwest–southeast shift of the minima between the two seasons and more realistic interannual differences over central and eastern Brazil.

Monthly distributions of RCM ensemble precipitation rates were spatially correlated with CMAP distributions over the Amazon region during all 6 months of the study, with PRED for May 1985 achieving the maximum correlation of 0.78. Considerable variability in modeled precipitation rates occurred between individual control simulations. However, common boundary forcing led to a convergence of results by May, expressed by high spatial correlations (between the individual simulations of precipitation distributions) over the Amazon region.

Comparison of modeled lower-tropospheric temperatures with NCEP reanalyses revealed a positive model bias of 1–3 K at 850 mb over tropical South America and a slight negative bias near the surface over eastern Brazil. This implies greater thermal stability of the lower troposphere for the mean state compared to NCEP reanalysis data, but judging by the validations of modeled precipitation for the region, this did not always translate into less frequent moist convection. The reason for excess RCM temperatures at 850 mb is not yet known, but the problem seems independent of the boundary forcing.

Convergence of meridional circulation at the ITCZ was stronger for the higher spatial resolution RCM fields than for NCEP reanalyses. MAM 1997 minus 1985 differences in meridional wind along 40°W were distinctly positive because of the more northerly position of the ITCZ in 1997, consistent with stronger southerlies to the south and weaker northerlies to the north. The downscaled predictions as well as the downscaled analyses captured the sense of these interannual changes in the ITCZ and related circulation. The RCM relative displacement of the ITCZ confluence at 40°W (about 3°) between these two seasons was similar to that shown by the corresponding NCEP reanalyses, but the coarse grid resolution of the latter somewhat obscures the distance of the actual shift.

The RCM is shown to be a promising tool for downscaling seasonal climate predictions. Some precipitation features simulated by the lower resolution GCM are improved by the advantages afforded by higher spatial resolution. Skillful SST predictions and/or better GCM circulation and humidity predictions are avenues for improving the end product, but the research shows that even ''perfect'' SST or observed atmospheric forcing do not translate into consistently realistic precipitation distributions. Improvements in the RCM convection and land surface treatment and in the mechanisms for nesting the model will perhaps lead to refinements in the quality of predicted climate fields represented on the 0.5° grid.

Acknowledgments. This research was part of a regional climate model intercomparison study organized in support of the International Research Institute for Climate Prediction (IRI). We gratefully acknowledge IRI support for this work and for providing rain gauge measurements over Brazil. LD and MF are partially supported by NSF Grant ATM-0089563 and by the NASA Climate and Earth Observing System Programs. NCEP reanalysis data was provided by Dr. Shyh Chen of the Experimental Climate Prediction Center at UCSD.

REFERENCES

Adler, R., C. Kidd, G. Petty, M. Morissey, and H. Goodman, 2001: Intercomparison of global precipitation products: PIP-3. *Bull. Amer. Meteor. Soc.,* **82,** 1377–1396.

Dastoor, A., and T. N. Krishnamurti, 1991: Landfall and structure of a tropical cyclone: Sensitivity of the model predictions to soil moisture parameterization. *Bound.-Layer Meteor.,* **55,** 345–380.

Deardoff, J., 1978: Efficient prediction of ground surface temperature and moisture with inclusion of a layer of vegetation. *J. Geophys. Res.,* **83,** 1889–1903.

Del Genio, A., M.-S. Yao, W. Kovari, and K.-W. Lo, 1996: A prognostic cloud water parameterization for global climate models. *J. Climate,* **9,** 270–304.

Druyan, L., M. Fulakeza, P. Lonergan, and M. Saloum, 2001: A regional model study of synoptic features over West Africa. *Mon. Wea. Rev.,* **129,** 1564–1577.

——, ——, and W. Thiaw, 2000a: Regional model simulations of African wave disturbances. *J. Geophys. Res.,* **105,** 7231–7255.

——, K. Shah, M. Chandler, and D. Rind, 2000b: GCM hindcasts of SST-forced climate variability over agriculturally intensive regions. *Climatic Change,* **45,** 279–322.

Fulakeza, M., L. Druyan, and T. Krishnamurti, 2002: A simple soil moisture scheme for climate simulations in the tropics. *Meteor. Atmos. Phys.,* **79,** 105–126.

Giorgi, F., and M. Marinucci, 1996: An investigation of the sensitivity of simulated precipitation to model resolution and its implication for climate studies. *Mon. Wea. Rev.,* **124,** 148–166.

——, and L. Mearns, 1999: Introduction to special section: Regional climate modeling revisited. *J. Geophys. Res.,* **104,** 6335–6352.

——, and X. Bi, 2000: A study of internal variability of a regional climate model. *J. Geophys. Res.,* **105,** 29 503–29 521.

Gutowski, W., and Coauthors, 2000: Project to Intercompare Regional Climate Simulations (PIRCS): Advancing the CLIVAR agenda. *CLIVAR Exchanges,* **5,** 13–15.

Hansen, J., and Coauthors, 1997: Forcings and chaos in interannual to decadal climate change. *J. Geophys. Res.,* **102,** 25 679–25 720.

Hartke, G., and D. Rind, 1997: Improved surface and boundary layer models for the GISS GCM. *J. Geophys. Res.,* **102,** 16 407–16 422.

Hastenrath, S., 1990: Prediction of Northeast Brazil rainfall anomalies. *J. Climate,* **3,** 353–365.

——, and L. Heller, 1977: Dynamics of climatic hazards in Northeast Brazil. *Quart. J. Roy. Meteor. Soc.,* **103,** 77–92.

——, and L. Greischar, 1993: Further work on the prediction of Northeast Brazil rainfall anomalies. *J. Climate,* **6,** 743–758.

Kistler, R., and Coauthors, 2001: The NCEP–NCAR 50-Year Reanalysis. *Bull. Amer. Meteor. Soc.,* **82,** 247–267.

Krishnamurti, T. N., S. Low-Nam, and R. Pasch, 1983: Cumulus parameterization and rainfall rates II. *Mon. Wea. Rev.,* **111,** 815–828.

——, A. Kumar, K. S. Yap, A. P. Dastoor, N. Davidson, and J. Sheng, 1990: Performance of high resolution mesoscale tropical prediction model. *Advances in Geophysics,* Vol. 32, Academic Press, 133–286.

Kuo, H., 1974: Further studies of the parameterization of the influence

of cumulus convection on large-scale flow. *J. Atmos. Sci.,* **31,** 1232–1240.

Liebmann, B., and C. Smith, 1996: Description of a complete (interpolated) outgoing longwave radiation dataset. *Bull. Amer. Meteor. Soc.,* **77,** 1275–1277.

——, J. Marengo, J. Glick, V. Kousky, I. Wainer, and O. Massambani, 1998: A comparison of rainfall, outgoing longwave radiation, and divergence over the Amazon Basin. *J. Climate,* **11,** 2898–2909.

Marengo, J., 1992: Interannual variability of surface climate in the Amazon basin. *Int. J. Climatol.,* **12,** 853–863.

Nobre, P., A. Moura, and L. Sun, 2001: Dynamic downscaling of seasonal climate prediction over Nordeste Brazil with ECHAM3 and NCEP's regional spectral models at IRI. *Bull. Amer. Meteor. Soc.,* **82,** 2787–2796.

Reynolds, R., and T. Smith, 1994: Improved global SST analyses. *J. Climate,* **7,** 929–948.

Rind, D., and J. Lerner, 1996: Use of on-line tracers as a diagnostic tool in general circulation model development. 1. Horizontal and vertical transport in the troposphere. *J. Geophys. Res.,* **101,** 12 667–12 683.

Ropelewski, C., 1999: The great El Niño of 1997–1998: Impacts on precipitation and temperature. *Consequences,* **5,** 17–26.

Rosenzweig, C., and F. Abramopoulous, 1997: Land-surface model development for the GISS GCM. *J. Climate,* **10,** 2040–2054.

Saulo, A., M. Nicolini, and S. Chou, 2000: Model characterization of the South American low-level flow during the 1997–1998 spring–summer season. *Climate Dyn.,* **16,** 867–881.

Takle, E., and Coauthors, 1999: Project to Intercompare Regional Climate Simulations (PIRCS): Description and initial results. *J. Geophys. Res.,* **104,** 19 443–19 461.

Uvo, C., C. Repelli, S. Zebiak, and Y. Kushnir, 1998: The relationships between tropical Pacific and Atlantic SST and Northeast Brazil monthly precipitation. *J. Climate,* **11,** 551–562.

Xie, P., and P. Arkin, 1997: Global precipitation: A 17-year monthly analysis based on gauge observations, satellite estimates, and numerical outputs. *Bull. Amer. Meteor. Soc.,* **78,** 2539–2558.